Journal of Thermal Science Vol.28, No.5 (2019) 993−1003

https://doi.org/10.1007/s11630-019-1116-6 **Article ID: 1003-2169(2019)05-0993-11**

Performance Assessment of Air-Cooled Steam Condenser with Guide Vane Cascade

ZHANG Xuelei*, LI Yunpeng, CHEN Haiping

School of Energy, Power and Mechanical Engineering, North China Electric Power University, Baoding 071003, China

Abstract: Ambient wind has an unfavourable impact on air-cooled steam condenser (ACSC) performance. A new measure to improve ACSC performance is proposed by setting a diffusion type guide vane cascade beneath the ACSC platform. The numerical models are developed to illustrate the effects of diffusion type guide vane cascade on ACSC performance. The simulation results show that this vane cascade can cause the increases in coolant flows across almost all fans due to its diffusion function and lower flow resistance. Meanwhile, the guide vane cascade also decreases the fan inlet temperatures because of the uniform flow field around the condenser cells. Comparing with the case without guide device, the overall heat transfer efficiency is increased by 11.2% for guide vane cascade case under the condition of 9 m/s. The heat transfer efficiency firstly enhances and then decreases with decreasing stagger angle of guide vane under a certain wind speed. The optimum stagger angle corresponding to the maximum heat transfer efficiency is about 65.5°. The heat transfer efficiency always enhances as increasing vane cascade height, and a vane cascade with 20 m to 30 m height may be suitable to the ACSC as considering the cost.

Keywords: air-cooled steam condenser, ambient wind, guide vane cascade, heat transfer

1. Introduction

Air-cooled steam condenser (ACSC) has been widely employed in power plant to cool the exhaust steam of turbine due to the characteristic of saving water. In ACSC, the exhaust steam directly releases heat to cooling air via the finned tubes. Obviously, ACSC's performance is susceptible to the environmental wind because it is exposed to the air [1-2].

Several literatures have revealed that ambient wind has an unfavourable impact on the performance of ACSC. The reasons that cause ACSC performance degradation mainly include reduction in fan performance, air backflow in condenser cell and hot air recirculation [3]. A low pressure area can be found beneath ACSC platform [4] when ambient wind flows through, which greatly decreases the cooling air flow of axial fan. Fan performance reduction may be the primary contributor to ACSC performance deterioration [5]. Hot air recirculation and backflow across the fans mainly depend on the ambient wind speed and its flow direction [6], and usually increase the temperature of cooling air under windy condition.

The proposed measures to restrain the disadvantage impacts of ambient wind on ACSC include setting guiding devices below the fan platform or in A-frame condenser cell [7-10], installing porous windbreak mesh below the fan platform [3,5,11], regulating blade angle and rotating speeds in windward fans [12-13], optimizing array of ACSC [14-15], and employing V-frame

Received: Aug 13, 2018 Corresponding author: ZHANG Xuelei E-mail: xueleizh@163.com

Nomenclature

ACSC	air-cooled steam condenser	v_{10}	wind speed at 10m height/m·s^{-1}
b	vane chord/m	v_f	axial velocity across a fan surface/m·s^{-1}
$C_{1\varepsilon}$, $C_{2\varepsilon}$, $C_{3\varepsilon}$	k-ε model constants	v_w	wind speed/m·s^{-1}
c_{pa}	isobaric specific heat of air/J·kg^{-1}·K^{-1}	V	volumetric flow rate/m^3·s^{-1}
C_i	inertial loss coefficient	z	height above the ground/m
e	specific energy/J·kg^{-1}	**Greek symbols**	
F_{ht}	heat transfer area/m^2	$1/\alpha_i$	viscous loss coefficient
FVE	fan volumetric efficiency	α_1	vane inlet angle/°
g	gravitational acceleration/m·s^{-2}	α_b	stagger angle/°
G_b	turbulence kinetic energy generation due to buoyancy/m^2·s^{-2}	ρ	Density/kg·m^{-3}
G_k	turbulence kinetic energy generation due to mean velocity gradients/m^2·s^{-2}	μ	dynamic viscosity/kg·m^{-1}·s^{-1}
h	specific enthalpy/J·kg^{-1}	ε	turbulence kinetic energy dissipation rate /m^2·s^{-3}
HTE	heat transfer efficiency	θ	camber angel/°
k	turbulence kinetic energy/m^2·s^{-2}	τ	stress tensor/J·m^{-3}
K_{ht}	heat transfer coefficiency/J·m^{-2}·K^{-1}	λ	thermal conductivity/W·m^{-1}·K^{-1}
l_h	heat exchanger thickness/m	σ	turbulent Prandtl number
$m_{a,i4}$	air mass flow rate through Fan (i,4)/kg·s^{-1}	ε_{i4}	heat transfer effectiveness of No.(i,4) exchanger
NTU	number of transfer units	ϖ	total pressure loss coefficient
p	Pressure/Pa	**Subscripts**	
Δp	pressure drop/Pa	1	inlet plane
Δp_f	fan pressure rise/Pa	2	outlet plane
$Q_{a,4}$	heat transfer rate of Column 4/W	a	air
$Q_{a,i4}$	heat transfer rate of No.(i,4) condenser cell /W	ftb	finned tube bundles
S_i	momentum source/N·m^{-3}	id	ideal
$t_{a,i4}$	temperature at the inlet of Fan (i,4)/°C	eff	effective
t_v	the steam turbine exhaust temperature/°C	t	turbulentn normal
t	cascade pitch/m	**Superscripts**	
T	Temperature/K	*	stagnation condition
v	air velocity/m·s^{-1}		

condenser cells with induced axial flow fans [16]. Setting guiding devices below the fan platform can not only introduce more coolant across the windward fans into condenser cells, but may form a uniform flow in A-frame condenser cells [7-8]. The air deflectors installed under the fan platform of ACCs are proposed, and the flow and temperature fields are analyzed for the air deflectors with various geometric parameters [9]. Similarly, a flow guiding device with arc-shape is installed inside the condenser cell to improve interior flow field as well as increase heat transfer rate of condenser cell [10]. The porous windbreak mesh that installs under the fan platform is also proposed to reduce the low pressure area at fan inlet, which may finally improve the windward fan performance as well as the whole ACSC performance [3,5,11]. It has been verified that the ambient wind has a more serious impact on windward fans, therefore increasing the volume flow rate of these fans by fan motor retrofit, fan blade angle adjustment [12] and rotating speeds enhancement [13] may restrain the disadvantage impacts of ambient wind and consquently improve the heat transfer characteristic of ACSC. In addition, the ACSC usually consists of the condenser cells with rectangular array no matter where the dominant wind comes from and how much the dominant wind speed is. Numerical simulations were conducted to investigate the effects of trapezoidal array [14] and circular array [15] of condenser cells in a 2×600 MW

power plant, aiming to restrain the adverse wind impacts. A novel V-frame condenser cell is also proposed in Ref. [16], and the simulation results show that it restrains the flow distortion through the fan and has better performance than conventional one.

The aforementioned studies all indicate that measures should be implemented to restrain the disadvantage effect of ambient wind on ACSC. An alternative option proposed in this study is to exploit a new guiding configuration, diffusion type guide vane cascade, to improve ACSC performance. Comparing to other guide device such as flat plates, this vane cascade not only has a lower flow resistance, but can increase static pressure of cooling air that derives from its velocity head under the effect of diffusion function, which may narrow the low pressure area under the platform and enhance the coolant flow rate through condenser cells. In present study, the numerical models are developed to illustrate the effects of diffusion type guide vane cascade on ACSC performance, and it is also suggested the optimum stagger angle and height corresponding to the maximum heat transfer rate.

2. Numerical Models

2.1 Physical model

The physical model follows up the previous work [17]. Fig. 1 shows the layout of an ACSC which consists of 56 condenser cells in a 600 MW power plant, and the ACSC releases 790 MW waste heat to the atmosphere under turbine heat acceptance (THA) condition. The focus of this numerical investigation is to compare the performance of condenser cells with and without diffusion type guide vane cascade under the same computational conditions. Ambient wind has roughly the same influence trend on each Column in air-cooled island under +X direction [4-5]. Therefore, in order to reduce grids and save computation time, only Column 4 section in the ACSC that consists of eight condenser cells is chosen to investigate the impacts of diffusion type guide vane cascade. Each condenser cell is a typical A-frame configuration with several finned tube bundles on two inclined sides and an axial flow fan on horizontal side. Fan's volume flow and static pressure are respectively 428 m^3/s and 66.1 Pa corresponding to fan rotational speed of 63 r/min.

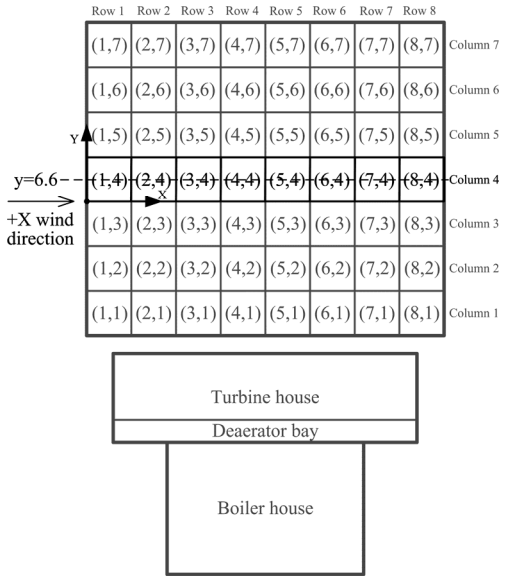

Fig. 1 Column 4 section in an ACSC

Fig. 2(a) presents the configuration and the installation position of the diffusion type guide vane cascade. The ACSC platform is 45 m high from the ground. The diffusion type guide vane cascade in Fig. 2(a) consists of 11 layers of vanes with a total height of 10 m. The vane profile is obtained on the basis of CDA profile by adjusting camber line, local thickness distribution, maximum deflection point position, and vane inlet and outlet angles, as shown in Fig. 3. The dimensions of the guide vane are listed in Table 1. Another guide device consisting of 11 layers of flat plates is also investigated to compare their impacts on ACSC performance, as shown in Fig. 2(b). These two guide devices have the same layer number, pitch and width. The focus of the manuscript is to investigate the effect of proposed guide vane cascade, so the flat plate structure is not optimized. The inclination angle of flat plate is selected as 45° that has been verified to possess better performance [7,9]. Fig. 4 shows the dimensions of the guide flat plates.

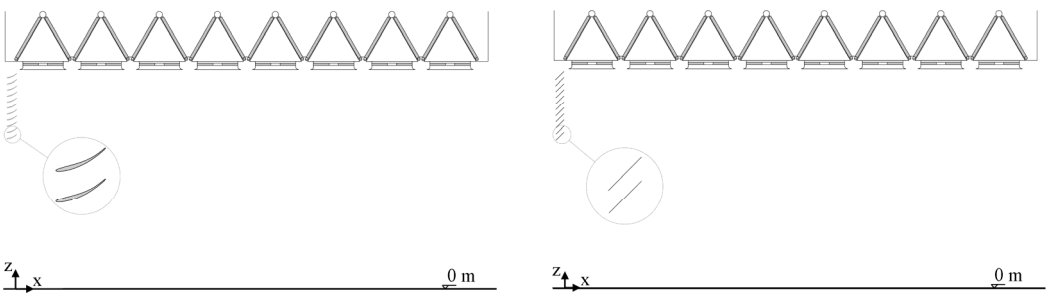

Fig. 2 Location of the guide devices: (a) diffusion type guide vane cascade, and (b) guide flat plates

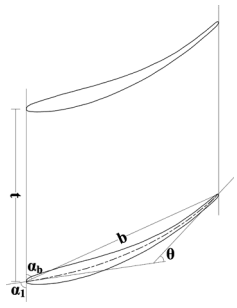

Fig. 3 Vane profile and notation.

Table 1 Cascade geometry

Cascade geometry		Value
Vane chord/m	b	1.22
Cascade pitch/m	t	1.0
Camber angel/°	θ	40
Vane inlet angle/°	α_1	82
Stagger angle/°	α_b	65.5

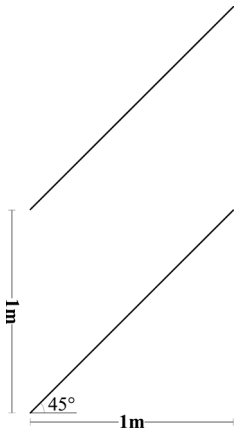

Fig. 4 The dimensions of guide flat plates

The computational domain has the total dimensions of 500 m×160 m×300 m (x×y×z). Gambit software is utilized to generate the computational grids by using tetrahedral unstructured grid approach. The verification of grid independence is achieved through the comparison of the total heat transfer rates under the grids consisting of about 2,650,200, 3,439,000, and 4,623,600 cells at the +X wind speed of 3 m/s. The deviation in total heat transfer rates between the two highest grid density solutions is only about 0.56%. The grid number of 3,439,000 is eventually employed in the current computations.

2.2 Numerical method and boundary conditions

The phenomenon of fluid flow is dominated by the conservation laws including mass, momentum, energy and extra turbulence transportation. The governing equations for the mass, momentum and energy conservations are as follows:

$$\frac{\partial(\rho v_i)}{\partial x_i}=0 \tag{1}$$

$$\frac{\partial(\rho v_i v_j)}{\partial x_j}=\frac{\partial}{\partial x_j}\left[\mu_{\text{eff}}\left(\frac{\partial v_i}{\partial x_j}+\frac{\partial v_j}{\partial x_i}\right)-\frac{2}{3}\mu_{\text{eff}}\frac{\partial v_k}{\partial x_k}\right] -\frac{\partial p}{\partial x_i}+\rho g_i+S_i \qquad (i,j,k=1,2,3) \tag{2}$$

$$\frac{\partial}{\partial x_i}\left(v_i\left(\rho e+p\right)\right)=\frac{\partial}{\partial x_i}\left(\lambda_{\text{eff}}\frac{\partial T}{\partial x_i}+v_j\left(\tau_{ij}\right)_{\text{eff}}\right) \tag{3}$$

where v_i is the velocity in the x_i direction; T is the temperature, p the pressure, and g_i is the gravitational acceleration in the x_i direction. In this model, g_i only exists in the -z direction. $e=h-p/\rho+v_i^2/2$ is the specific energy, where h is the specific enthalpy; $\mu_{\text{eff}}=\mu+\mu_t$ is the effective dynamic viscosity, where μ and μ_t are the dynamic viscosity and turbulent dynamic viscosity respectively. τ_{eff} is the stress tensor; λ_{eff} is the effective thermal conductivity; S_i is the momentum source and equals to the pressure drop per flow passage length through the tube bundles, and ρ is air density.

The effect of turbulence on the flow field is included in the application of the standard k-ε turbulent model. Robustness, economy, and reasonable accuracy for a wide range of turbulent flows explain the popularity in industrial flow and heat transfer simulations of the standard k-ε turbulent model [18].

$$\frac{\partial}{\partial x_i}\left(\rho k v_i\right)=\frac{\partial}{\partial x_j}\left[\left(\mu+\frac{\mu_t}{\sigma_k}\right)\frac{\partial k}{\partial x_j}\right]+G_k+G_b-\rho\varepsilon \tag{4}$$

$$\frac{\partial}{\partial x_i}\left(\rho\varepsilon v_i\right)=\frac{\partial}{\partial x_j}\left[\left(\mu+\frac{\mu_t}{\sigma_\varepsilon}\right)\frac{\partial \varepsilon}{\partial x_j}\right] +C_{1\varepsilon}\frac{\varepsilon}{k}\left(G_k+C_{3\varepsilon}G_b\right)-C_{2\varepsilon}\rho\frac{\varepsilon^2}{k} \tag{5}$$

where k and ε are the turbulence kinetic energy and its rate of dissipation; σ_k and σ_ε are the turbulent Prandtl number for k and ε; G_k represents the generation of turbulence kinetic energy due to the mean velocity gradients, and G_b is the generation of turbulence kinetic energy due to the buoyancy. The model constants have the following default values, $C_{1\varepsilon}$=1.44, $C_{2\varepsilon}$=1.92, $C_{3\varepsilon}$=1, σ_k=1.0, σ_ε=1.3.

The convective terms in the momentum, energy and turbulence equations are discretized by using the first-order upwind schemes that is computationally more stable compared to the second-order upwind scheme. The SIMPLE algorithm for a steady-state solution is employed during the numerical simulation. The coolant air is considered as an incompressible fluid [19], and

incompressible variable density model is introduced to simulate the effect of buoyancy force on cooling air.

The finned tube bundles are handled by the porous media model in FLUENT. The flow resistance of coolant across condenser cell is obtained from the manufacturer and is described as

$$\Delta p_{\mathrm{ftb}} = 16.1 v_{\mathrm{ftb}}^2 + 17.4 v_{\mathrm{ftb}} \tag{6}$$

where Δp_{ftb} and v_{ftb} are pressure drop and air velocity across the finned tube bundles, respectively.

Fluent simulates the flow resistance of coolant by using the momentum source term S_{i} which includes the viscous resistance and inertial resistance term as

$$S_{\mathrm{i}} = -\frac{\Delta p_{\mathrm{ftb}}}{l_{\mathrm{h}}} = -\left(\frac{\mu}{\alpha_{\mathrm{i}}} v_{\mathrm{i}} + C_{\mathrm{i}} \frac{1}{2} \rho_{\mathrm{a}} | \boldsymbol{v} | v_{\mathrm{i}} \right) \tag{7}$$

where C_{i} is the inertial loss coefficient; $1/\alpha_{\mathrm{i}}$ is the viscous loss coefficient, and the footnote i represents the individual Cartesian directions, ρ_{a} air density, and l_{h} is the thickness of heat exchanger, 0.219 m.

Based on Eqs. (6) and (7), C_{n} is set to 139.6, and $1/\alpha_{\mathrm{n}}$ is set to 4,465,730. The footnote n denotes the normal direction to the finned tube bundles. The temperature of finned tube bundles is considered to equal to the value at which exhaust steam condenses because the thermal conduction resistance is negligible. In the numerical models, the porous zone and steam duct surface are set to the uniform temperature of 46.6℃. The axial fan is modeled as a pressure jump surface, and the pressure rise Δp_{f} of coolant across the surface is related to the fan's axial velocity v_{f}. According to fan's performance curve supplied by manufacturer, Δp_{f} is described as a polynomial form of v_{f},

$$\Delta p_{\mathrm{f}} = 144.8 - 5.86 v_{\mathrm{f}} - 0.81 v_{\mathrm{f}}^2 \tag{8}$$

To simplify the simulation of axial flow fans, the tangential velocity and radial velocity are neglected due to the low fan rotation speed. The experiment found that both the tangential velocity and radial velocity are small as compared to axial velocity [20].

The velocity-inlet boundary condition is designated to the windward plane of the computational domain on which the velocity profile v_{w} of ambient wind is appointed as

$$v_{\mathrm{w}} = v_{10} \left(\frac{z}{10} \right)^x \tag{9}$$

where v_{10} represents the ambient wind speed at the height of 10 m above ground; z is the height above the ground, and the exponent x denotes the ground roughness and atmospheric stability. Considering the geographical location of power plant, x is appointed as 0.2 in this paper.

The effects of ambient wind under the speeds of 3 m/s, 6 m/s and 9 m/s are simulated in the manuscript. Outflow boundary condition is applied on the downstream plane of computational domain where the diffusion flux in the normal direction is zero. All surfaces of computational domain except windward and downstream planes are assigned to symmetry boundary conditions. Especially under windless condition, pressure-inlet condition is employed on all surfaces of computational domain except top and bottom planes, while pressure-outlet condition is applied on the top plane. Wall boundary conditions are designated to the surfaces such as ground, wind break wall, steam duct and guide devices. The numerical models are simulated for THA condition, and the main operation parameters of ACSC are presented in Table 2.

Table 2 Main operation parameters of ACSC under THA condition

Items	Value
Atmospheric temperature/°C	14
Atmospheric pressure/Pa	86,900
Exhaust temperature/°C	46.6
Exhaust flow/kg·s^{-1}	349.4
Average heat duty of condenser cell/MW	14.1

2.3 Data reduction

The manuscript employs the fan volumetric efficiency (FVE) and heat transfer efficiency (HTE) to assess the ACSC performance under windy condition. The *FVE* is defined as

$$FVE = \frac{V_{\mathrm{windy}}}{V_{\mathrm{windless}}} \tag{10}$$

where V_{windy} and V_{windless} are respectively fan volumetric flow rates under windy condition and windless condition.

The *HTE* is defined as

$$HTE = \frac{Q_{\mathrm{a}}^{\mathrm{windy}}}{Q_{\mathrm{a}}^{\mathrm{windless}}} \tag{11}$$

where $Q_{\mathrm{a}}^{\mathrm{windy}}$ and $Q_{\mathrm{a}}^{\mathrm{windless}}$ are respectively heat transfer rates under windy condition and windless condition.

As far as the condenser cells in Colume 4, the overall heat transfer rate $Q_{\mathrm{a,4}}$ is calculated by [21]

$$Q_{\mathrm{a,4}} = \sum_{i=1}^{8} Q_{\mathrm{a,i4}} = \sum_{i=1}^{8} m_{\mathrm{a,i4}} c_{\mathrm{pa}} \varepsilon_{\mathrm{i4}} \left(t_{\mathrm{v}} - t_{\mathrm{a,i4}} \right) \tag{12}$$

$$\varepsilon_{\mathrm{i4}} = 1 - e^{-NTU_{\mathrm{i4}}} \tag{13}$$

$$NTU_{\mathrm{i4}} = \frac{K_{\mathrm{ht,i4}} F_{\mathrm{ht,i4}}}{m_{\mathrm{a,i4}} c_{\mathrm{pa}}} \tag{14}$$

where Q_{a} denotes heat transfer rate; m_{a} is air mass flow predicted by numerical simulation; t_{a} is the inlet temperature of condenser cell; t_{v} represents the temperature of exhaust steam; c_{pa} is the specific heat of

air at constant pressure; ε is the heat transfer effectiveness; *NTU* represents the number of transfer units; K_{ht} is the heat transfer coefficiency; F_{ht} represents the heat transfer area and the footnote i4 denotes No.(i,4) condenser cell.

The ambient wind will alter the air mass flow and inlet temperature of condenser cell. In this manuscript, the turbine back pressure and its corresponding saturation temperature are assumed to remain unchanged under windy condition, so the overall heat transfer rate will be altered according to Eq. (12). By means of CFD simulations, the air mass flow and inlet temperature of the condenser cell can be obtained. On this basis, the overall heat transfer rate is calculated via Eqs. (12)-(14).

2.4 Validation of the numerical model

The performances of Column 4 under three typical operating modes, including summer mode, THA mode and blocking mode are numerically investigated at the prevailing wind direction with a wind speed of 3 m/s. The numerical models are validated by comparing the average fan volumetric flow rate and heat transfer rate of condenser cells. The relative errors of fan volumetric flow rate under summer mode, THA mode and blocking mode are respectively 0.22%, 0.17% and 0.26%. In addition, the relative errors of heat transfer rate under these three operation modes are respectively 0.26%, 0.19% and 0.28%. The consistency of fan volumetric flow rate as well as heat transfer rate indicates that the numerical models are reliable enough for the purpose of this investigation.

3. Results and Discussion

3.1 Fan inlet air temperature

The fan inlet air temperature may indicate the seriousness of hot air recirculation, backflow and vortex flow in condenser cells. The fan inlet air temperatures of all condenser cells in Column 4 at the wind speed of 9 m/s are demonstrated as an example, and the temperature contours are presented in Fig. 5. The differences in fan inlet air temperatures among the cases without guide device, with guide vane cascade and with guide flat plates can be clearly observed. The temperatures at fans inlets or inside condenser cells are obviously high for without guide device case. In addition, the ambient wind has obvious effect on inlet air temperatures of windward and interior cells, while it has little impact on inlet air temperatures of downstream cells, as shown in Fig. 6. Fan(1,4) is the first to be impacted by the approaching wind compared to the other condenser cells further downstream of the Column 4 section. Air inlet temperatures of windward condenser cells have a notable decrease as considering guide vane cascade or guide flat plates. Especially for Fan(1,4), the inlet temperature decreases from about 15.1°C to 14.0°C as considering guide vane cascade. Fig. 6 also shows that the guide vane cascade and the guide flat plates exhibit almost the equivalent function in fan inlet air temperature drop. Fig. 7 presents the streamline plots at the profile of y=6.6 m. It can be found that the drop in the air inlet temperatures results from the restrained vortex flow at the inlet of windward condenser cells as considering guide devices. Therefore, the uniform flow field around the condenser cells is formed with the help of guide function of vane cascade.

3.2 Fan volumetric efficiency

Fig. 8 presents the *FVE* of condenser cells in Column 4 under +X wind conditions. It can be seen that the *FVE* is the worst for the windward fans, especially for Fan(1,4). *FVE* of Fan(1,4) is only 58.0% under a wind speed of 9 m/s. The area affected by ambient wind increases as the wind gets stronger and stronger. For instance, most of the upstream fans between rows 1 to 4 are severely affected as the wind speed exceeds 6 m/s. Fig. 9 illustrates the

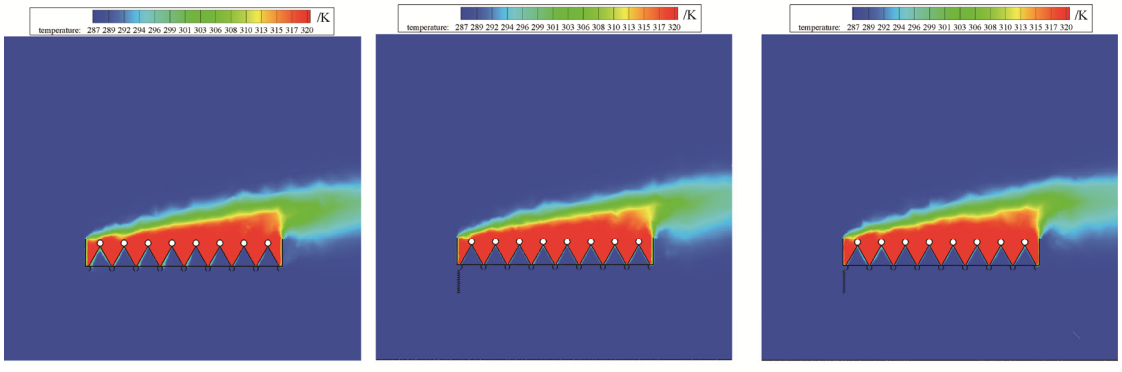

(a) (b) (c)

Fig. 5 Temperature plots at the profile of y=6.6 m under the wind speed of 9 m/s (a) without guide device, (b) with guide vane cascade, and (c) with guide flat plates

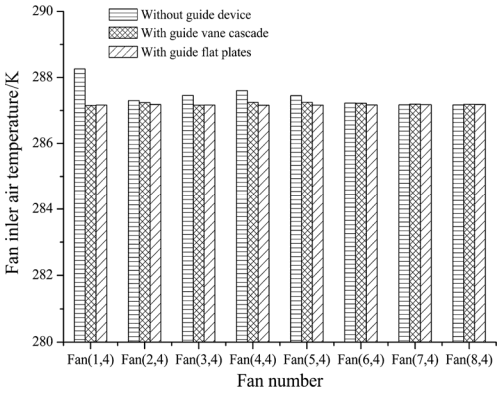

Fig. 6 Fan inlet air temperature at the +X wind speed of 9 m/s

significant static pressure drop under the ACSC platform by means of static pressure contour plots at the profile of y=6.6 m. This low pressure region consequently results in the *FVE* reduction.

Different guide devices are investigated to compare their individual influence on the performance of Column 4. Fig. 8 shows that the performance of fans in Column 4 remains approximately unchanged under windless condition as considering guide devices, whereas the volumetric efficiency of almost all fans is progressively improved by guide devices under windy conditions and even shows performances surpassing 100%, especially for windward fans. The *FVE* of Fan(1,4) increases from 58.0% to 112.5% for guide vane cascade under a wind speed of 9 m/s. This occurs since the region beneath the fan platform experiences an increase in static pressure, due to the diffusion function of guide vane cascade. As ambient wind flows through the diffusion type guide vane cascade, the velocity head of wind is converted to the pressure head. Therefore, the low pressure area under the platform is shrunk by adding the diffusion type guide vane cascade as shown in Figs. 9 and 10, which consequently improves the fans performances. However, the performances of downstream fans between rows 7 to 8 decrease slightly as considering guide devices. As shown in Fig. 7, the cooling air drawn in the Fan(7,4) and Fan(8,4) needs to flow around the guide devices, which may cause the reduction in volumetric flow through these fans.

The overall volumetric flow of fans in Column 4 is shown in Fig. 11. The volumetric flow rate can be observed to increase markedly as considering the flow guide devices. The guide vane cascade shows a better performance than the specified guide flat plates in overall volumetric flow. Flowing resistance plays a significant role in the performance of guide devices, and the total pressure loss coefficient is employed to investigate the flowing resistance through these guide devices, as

$$\varpi=\frac{p_1^*-p_2^*}{p_2^*-p_2} \tag{15}$$

where ϖ is the total pressure loss coefficient; subscript 1 denotes the inlet plane; subscript 2 denotes the outlet plane; superscript * denotes stagnation condition.

As shown in Figs. 11 and 12, the resistance flowing through the guide vane cascade is greatly lower than that through the specified guide flat plates, which is helpful to improve the fans overall volumetric flow, especially under higher ambient wind speed conditions.

3.3 Heat transfer efficiency

The ACSC is mainly responsible for removal of the thermal duty of exhaust steam in power plant. Therefore, it is of great importance to investigate the heat transfer performance under windy condition. Fig. 13 shows the overall *HTE* of Column 4, subject to +X wind direction. It is found that the performance of Column 4 section deteriorates with an increase in wind speed. The heat released by condenser cells sharply declines when the wind speed exceeds 3 m/s, and HTE drops to 0.92 with the further augment of wind speed up to 9 m/s. Obviously, both the guide vane cascade and guide flat plates

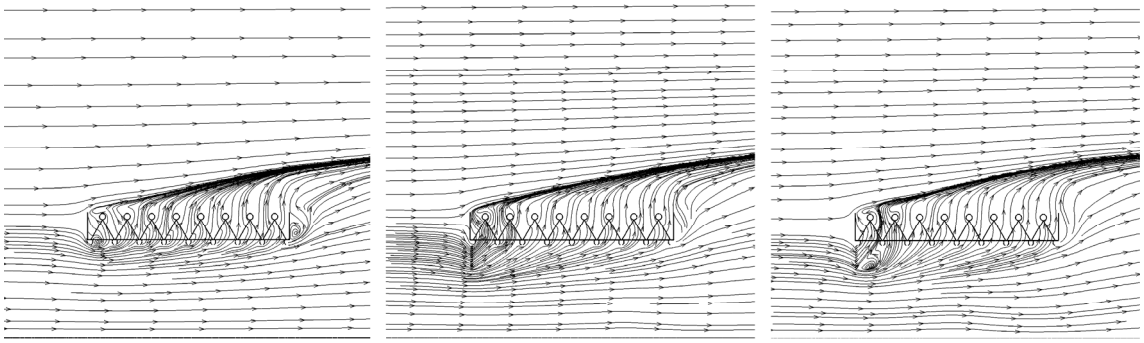

(a) (b) (c)

Fig. 7 Streamline plots at the profile of y=6.6 m under the wind speed of 9 m/s (a) without guide device, (b) with guide vane cascade, and (c) with guide flat plates

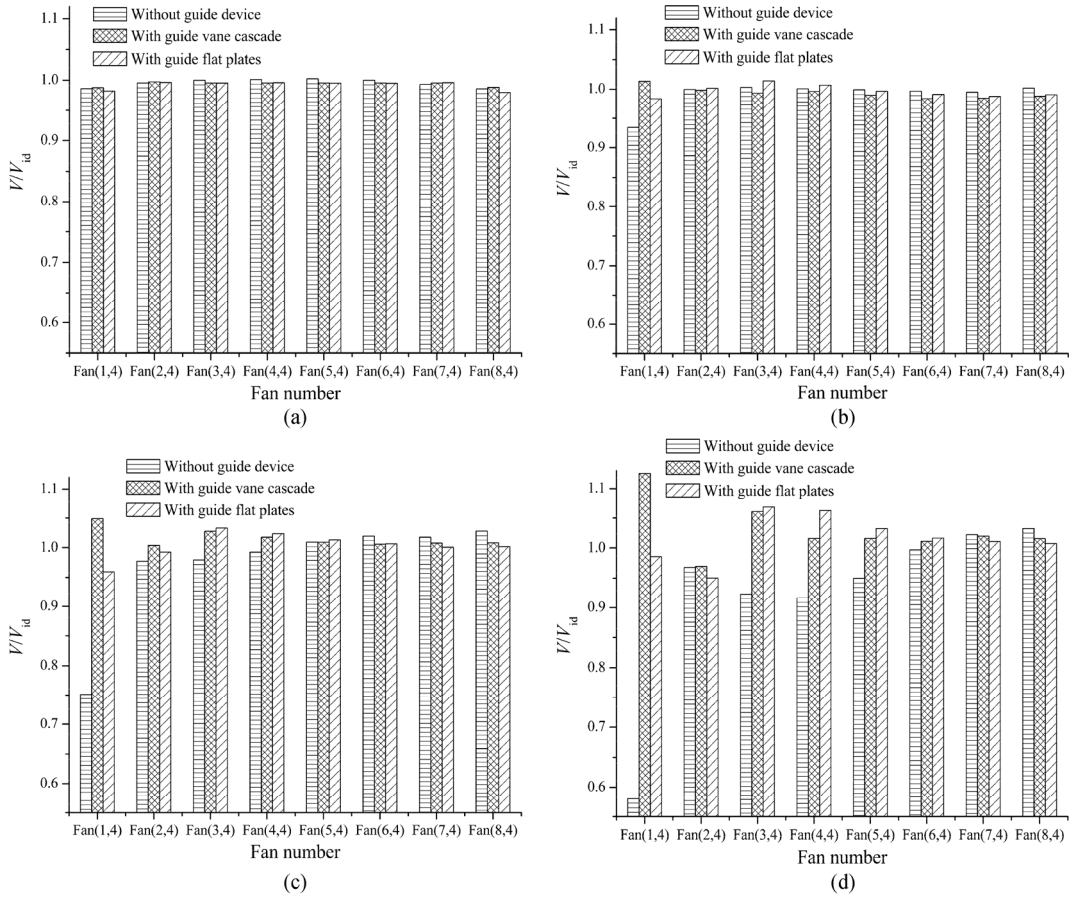

Fig. 8 *FVE* of each fan at wind speeds of (a) 0 m/s, (b) 3 m/s, (c) 6 m/s, and (d) 9 m/s

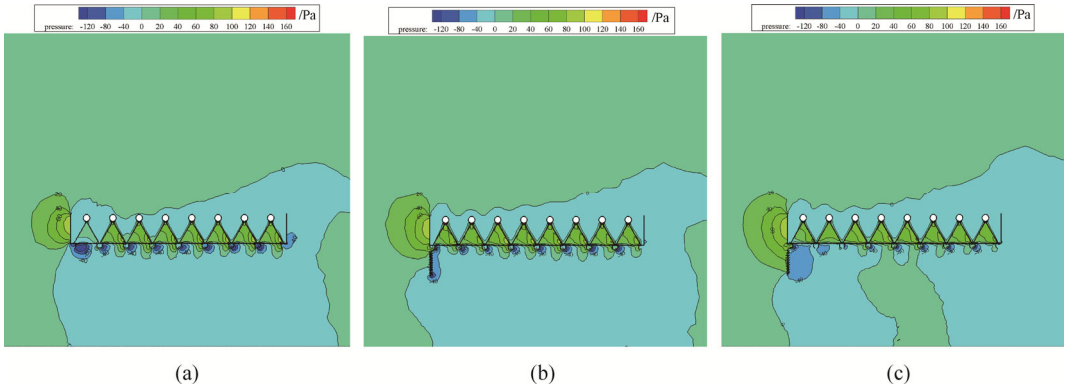

Fig. 9 Static pressure plots at the profile of y=6.6 m under a wind speed of 9 m/s (a) without guide device, (b) with guide vane cascade, and (c) with guide flat plates

improve the *HTE* of condenser cells in Column 4 under windy conditions. This improvement in heat transfer performance varies more widely at higher wind speeds. Comparing with the case without guide device, the overall *HTE* is increased by 11.2% for guide vane cascade case and by 10.0% for guide flat plates case under the condition of 9 m/s. In addition, there is no significant difference in *HTE* between without guide device case and guide vane cascade case under windless condition, which indicates that the guide vane cascade would not decrease the ACSC performance under windless condition. The guide vane cascade shows better performance than the specified guide flat plates, and the *HTE* improvement indicates that guide vane cascade is an effective means to restrain the disadvantage effects of ambient wind.

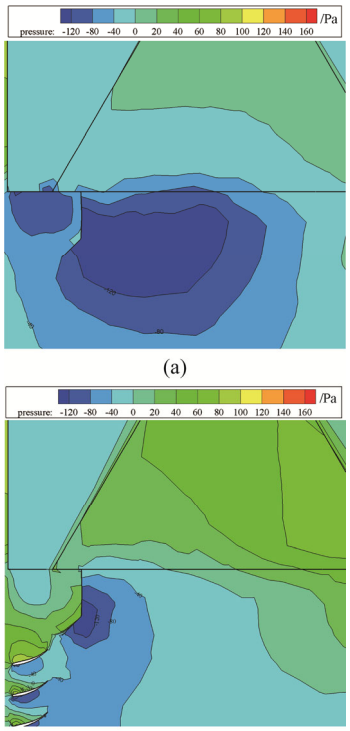

Fig. 10 Local magnification for static pressure plots at Fan(1,4) inlet under a wind speed of 9 m/s (a) without guide device, and (b) with guide vane cascade

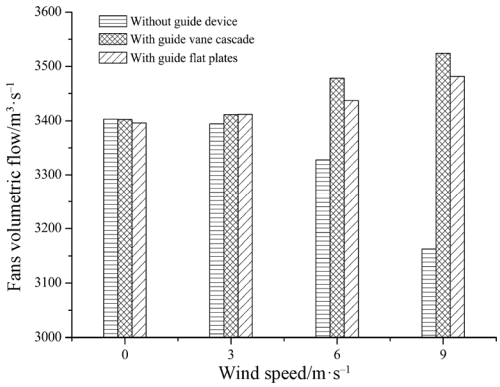

Fig. 11 Overall fans volumetric flow

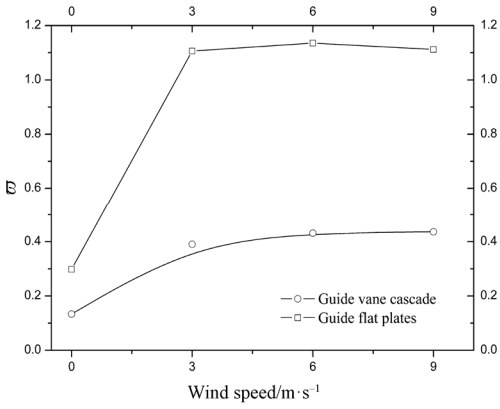

Fig. 12 Total pressure loss coefficient

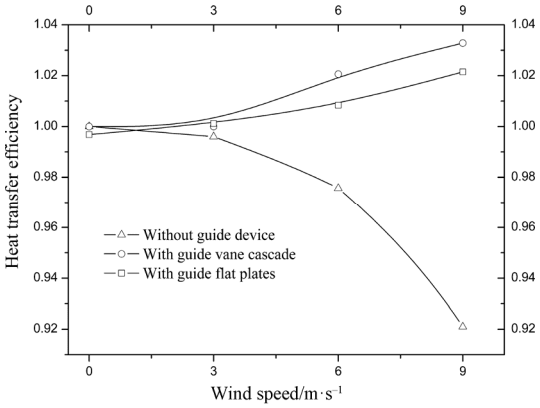

Fig. 13 *HTE* for Column 4 under windy conditions

4. Optimization of Guide Vane Cascade

For the second set of simulations, we fixed the ambient wind condition the same as Section 3 to analyze the effects of stagger angle and height of guide vane cascade on ACSC performance.

4.1 The effects of stagger angle

The effects of guide vane stagger angle on the *HTE* of Column 4 are evaluated at different stagger angles of 50.5°, 65.5°, 80.5°, 95.5°, and 110.5°, as shown in Fig. 14. A guide vane cascade with 10 m height is employed to conduct the simulations. The *HTE* vs stagger angle is shown in Fig. 15. Under the conditions of windless or lower wind speed, the stagger angle has little effect on the overall *HTE* of Column 4. However, under a higher wind speed such as 6 m/s and 9 m/s, the overall *HTE* is greatly affected by stagger angle. As shown in Fig. 14, the guiding effect of vane cascade may become stronger with decreasing stagger angle. As a result, more and more cooling air could be guided into the condenser cells located on the top of guide vane cascade, which improves the overall *HTE* of Column 4. But on the other hand, too small stagger angle greatly alters the wind flow direction, and it may cause the flow resistance increase and consequently decrease volumetric flow through fans. Therefore, the overall *HTE* of Column 4 firstly enhances and then decreases with decreasing stagger angle under a certain wind speed. Fig. 15 indicates that the optimum stagger angle corresponding to the maximum *HTE* is about 65.5°.

4.2 The effects of vane cascade height

The *HTE* of Column 4 is respectively calculated for the guide vane cascade with the height of 10 m, 20 m, 30 m and 40 m, as shown in Fig. 16. Under the conditions of windless or lower wind speed, the vane cascade height also has little effect on the overall HTE of Column 4, while it would exert an influence under the higher wind speed conditions. Fig. 17 compares the streamline plots

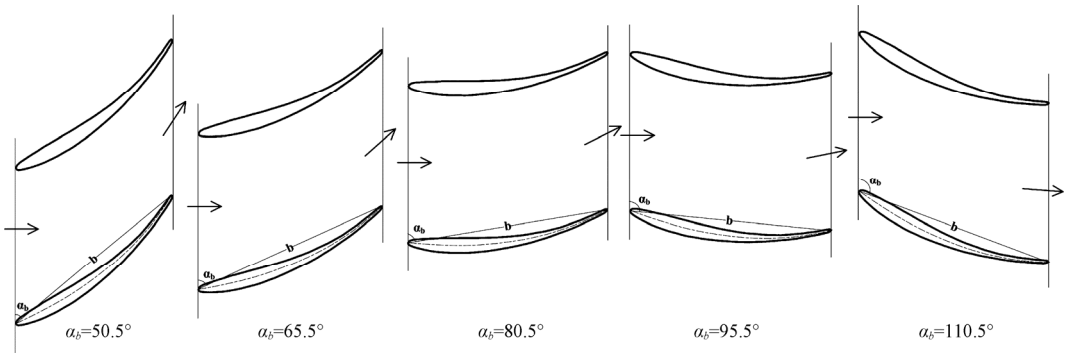

Fig. 14 The stagger angle of guide vane cascade

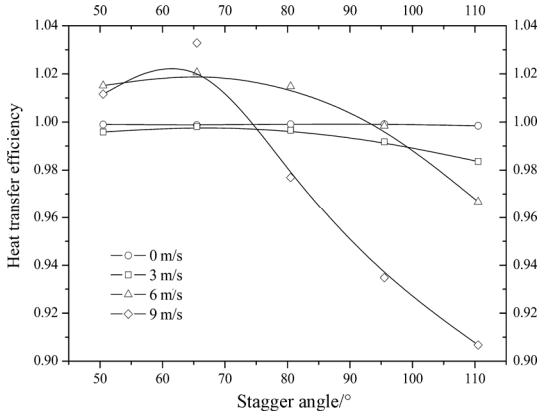

Fig. 15 The effects of stagger angle on *HTE*

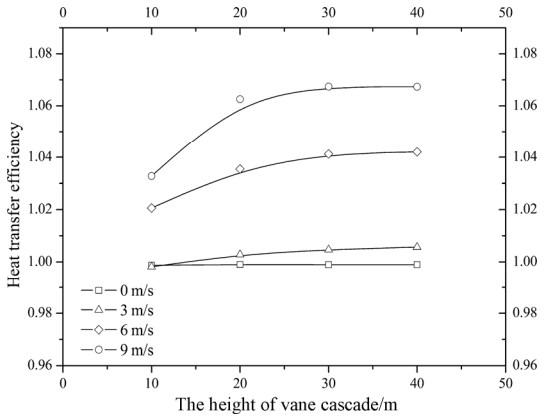

Fig. 16 The effects of vane cascade height on *HTE*

for Column 4 with vane cascade of 20 m and 40 m height under a wind speed of 9 m/s. It denotes that the vane cascade with higher height can guide cooling air into more condenser cells. For instance, the vane cascade with 40 m height can guide cooling air into upwind six condenser cells, while the vane cascade with 20 m height only guides air into three condenser cells. As a result, the *HTE* enhances with increasing vane cascade height under a certain wind speed. It is also found that the growth rate of *HTE* becomes slow as the vane cascade height exceeds 30 m. Consequently, the vane cascade with 20 m to 30 m height may be suitable to the ACSC as considering the cost.

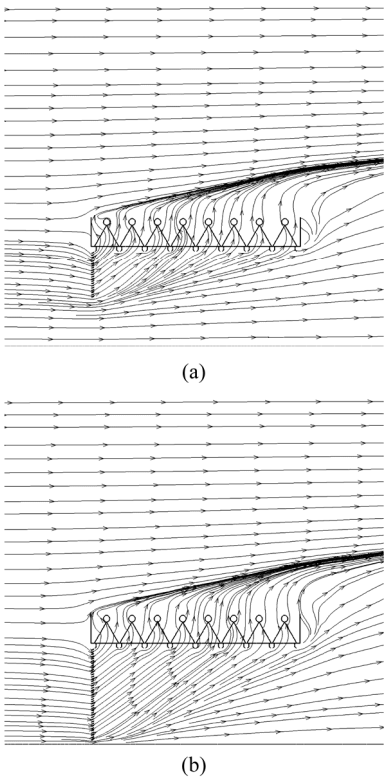

Fig. 17 Streamline plots at the profile of y = 6.6 m under a wind speed of 9 m/s (a) with 20 m height of vane cascade and (b) with 40 m height of vane cascade

5. Conclusions

A new measure to improve ACSC performance is proposed by setting a diffusion type guide vane cascade under the platform. The numerical models are developed to illustrate the effects of diffusion type guide vane cascade on ACSC performance, and the optimum stagger angle and height corresponding to the maximum heat transfer rate are also suggested.

(1) The reasons that cause ACSC performance degradation under windy condition include air temperature increase at fan inlet and cooling air flow reduction across axial fan. The simulation results show

that the diffusion type guide vane cascade can cause the drops in fans inlet air temperatures as well as the increases in coolant flows across almost all fans. This occurs owing to the uniform flow field around the condenser cell and static pressure rise in the region beneath the platform, due to the guide and diffusion functions of guide vane cascade. Comparing with the case without guide device, the overall *HTE* is increased by 11.2% for guide vane cascade case under the condition of 9 m/s.

(2) The guide vane cascade shows better performance than the specified guide flat plates due to the lower resistance flowing through guide vane cascade.

(3) The overall *HTE* of Column 4 firstly enhances and then decreases with decreasing stagger angle under a certain wind speed. The optimum stagger angle corresponding to the maximum *HTE* is about 65.5°.

(4) The *HTE* enhances with increasing vane cascade height under a certain wind speed, while its growth rate becomes slow as the vane cascade height exceeds 30 m. Consequently, the vane cascade with 20 m to 30 m height may be suitable to the ACSC as considering the cost.

Acknowledgments

This work was supported by the National Key Research and Development Program of China (2018YFB0604302-02); and the National Natural Science Foundation of China (No.51606066).

References

[1] Butler C., Grimes R., The effect of wind on the optimal design and performance of a modular air-cooled condenser for a concentrated solar power plant. Energy, 2014, 68: 886–895.

[2] Dang C., Jia L., Yang L., Effects of acoustic barriers and crosswind on the operating performance of evaporative cooling tower groups. Journal of Thermal Science, 2016, 25(6): 532–541.

[3] Bustamante J.G., Rattner A.S., Garimella S., Achieving near-water-cooled power plant performance with air-cooled condensers. Applied Thermal Engineering, 2016, 105: 362–371.

[4] Zhang X.L., Chen H.P., Effects of windbreak mesh on thermo-flow characteristics of air-cooled steam condenser under windy conditions. Applied Thermal Engineering, 2015, 85: 21–32.

[5] Owen M.T.F., Kröger D.G., The effect of screens on air-cooled steam condenser performance under windy conditions. Applied Thermal Engineering, 2010, 30(16): 2610–2615.

[6] Liu P.Q., Duan H.S., Zhao W.L., Numerical investigation of hot air recirculation of air-cooled condensers at a large power plant. Applied Thermal Engineering, 2009, 29(10): 1927–1934.

[7] Gao X.F., Zhang C.W., Wei J.J., Yu B., Performance predication of an improved air-cooled steam condenser with deflector under strong wind. Applied Thermal Engineering, 2010, 30(17/18): 2663–2669.

[8] Yang L.J., Du X.Z., Yang Y.P., Improvement of thermal performance for air-cooled condensers by using flow guiding device. Journal Enhanced Heat Transfer, 2012, 19: 63–74.

[9] Huang X.W., Chen L., Kong Y.Q., Effects of geometric structures of air deflectors on thermo-flow performances of air-cooled condenser. International Journal of Heat and Mass Transfer, 2018, 118: 1022–1039.

[10] Zhang W.X., Yang L.J., Du X.Z., et al., Thermo-flow characteristics and air flow field leading of the air-cooled condenser cell in a power plant. Science China, 2011, 54(9): 2475–2482.

[11] Gu H.F., Zhe Z., A numerical study on the effect of roof windbreak structures in an air-cooled system. Applied Thermal Engineering, 2015, 90: 684–693.

[12] He W.F., Dai Y.P., Zhu S., et al., Influence from the blade installation angle of the windward axial fans on the performance of an air-cooled power plant. Energy, 2013, 60: 416–425.

[13] He W.F., Dai Y.P., Han D., et al., Influence from the rotating speed of the windward axial fans on the performance of an air-cooled power plant. Applied Thermal Engineering, 2014, 65(1/2): 14–23.

[14] Yang L.J., Wang M.H., Du X.Z., Trapezoidal array of air-cooled condensers to restrain the adverse impacts of ambient winds in a power plant. Applied Energy, 2012, 99: 402–413.

[15] Kong Y.Q., Wang W.J., Huang X.W., et al., Circularly arranged air-cooled condensers to restrain adverse wind effects. Applied Thermal Engineering, 2017, 124: 202–223.

[16] Chen L., Yang L.J., Du X.Z., Novel air-cooled condenser with V-frame cells and induced axial flow fans. International Journal of Heat and Mass Transfer, 2018, 117: 167–182.

[17] Zhang X.L., Wu T.T., Effects of diffuser orifice plate on the performance of air-cooled steam condenser. Applied Thermal Engineering, 2016, 98: 179–188.

[18] Versteeg H.K., Malalasekera W., An introduction to computational fluid dynamics: the finite volume method. Pearson Education Limited, Second edition, England, 2007.

[19] Wang M., Wang J., Wang J.J., et al., Contrastive analysis of cooling performance between a high-level water collecting cooling tower and a typical cooling tower. Journal of Thermal Science, 2018, 27(1): 39–47.

[20] Yang L.G., Use of experimental data to generate swirl velocity in the FLUENT fan model. University of Windsor, 2002.

[21] Yang S.M., Heat transfer. Higher Education Press, Beijing, 2006.